



Monte Carlo simulations of self-assembling star-block copolymers in dilute solutions

Alessandro Patti

Soft Condensed Matter, Debye Institute for NanoMaterials Science, Utrecht University, Princetonplein 5, 3584 CC Utrecht, The Netherlands

ARTICLE INFO

Article history:

Received 27 January 2010

Received in revised form 11 March 2010

Accepted 14 March 2010

Available online 23 March 2010

Keywords:

Self-assembly

Star-block copolymers

Micellization

Critical micellar concentration

ABSTRACT

Computer simulations have been performed to analyze the aggregation behavior in dilute solutions of star-block copolymers of the type $(AB)_n$ in a selective solvent for the B block. We found spontaneous aggregation of single stars and formation of roughly spherical aggregates. By changing the solvophobic/solvophilic length ratio of the two blocks, and keeping the total arm length constant, we observed significant changes in the resulting micellar properties, such as the critical micellar concentration (CMC) and aggregation number. More specifically, by increasing the length of the solvophobic A block, we observe micellization at higher temperatures; whereas by increasing the length of the solvophilic B block, we observe micellization at very low temperatures. We also found a dependence of the CMC on the temperature which is in very good agreement with a recent theoretical description based on a simple thermodynamic framework. We compare our results with this theory and predict the enthalpy and entropy of micellization as a function of the temperature.

© 2010 Elsevier B.V. All rights reserved.

1. Introduction

The phase and aggregation behavior of amphiphilic block copolymers has been of remarkable scientific interest for over fifty years because of their distinctive physical properties, which are essential in a significant number of industrial applications [1]. However, most of the scientific output has focused mainly on linear diblock or triblock copolymers [2,3], leaving other more complex structures on a secondary level. In the last two decades, the development of several experimental techniques to synthesize star-like copolymers [4–8] and, in particular, advances in controlled radical polymerizations, such as atom transfer radical polymerization [9–12], has triggered an increasing interest toward intriguing non-linear architectures, such as heteroarm, miktoarm, and star-block copolymers, which consist of several arms radiating from a common central core. More specifically, heteroarm and miktoarm copolymers, concisely denoted as A_nB_n and A_nB_m , respectively, consist of n arms containing only units of type A , and the remaining (n or m) arms containing only units of type B . Star-block copolymers, usually referred to as $(AB)_n$, may be described as star polymers where each of the arms is a linear block copolymer [13]. They consist of n arms with a bridging block of A units attached to the central core, and a terminal block of B units. The structural properties of star-like copolymers and in particular their ability to self-assemble, make them of significant interest as drug delivery vehicles [14–19],

polymer films [20], and in catalysis [21–23]. For instance, star-block copolymers made of biocompatible poly(ethylene oxide) arms find important applications in biomedical and pharmaceutical areas [24], and they are especially promising for functionalization [25]. There are three general ways of synthesis which are usually referred to as *core first*, *arm first*, and *coupling onto* methods [26]. In the *core first* approach, a multifunctional initiator starts the simultaneous polymerization of the arms; the *arm first* approach involves the reaction between a linear copolymer and a multifunctional cross-linker; the last technique can be considered as a combination of the other two, and involves a reaction between a functionalized polymer and a multifunctional linking agent [27].

Star-like copolymers show an interesting micellization behavior which may deviate from that of the analogous linear block copolymers with either the same molecular weight or the same arm block length [28–30]. By means of static and dynamic light scattering and viscometry, Voulgaris et al. found that the micellization properties of polystyrene/poly(2-vinylpyridine) star copolymer in a selective solvent for polystyrene (PS), are significantly different from those of the corresponding diblock copolymer having the same block lengths as those of the star arms [29]. In particular, the star-block copolymer exhibits a much higher critical micellar concentration (CMC) and a lower aggregation number with respect to the linear copolymer. By applying the same experimental techniques, Mountrichas et al. studied the aggregation behavior of star-block copolymers made of PS and polyisoprene blocks in PS-selective solvents [30]. These authors concluded that such stars self-assemble in micelles of smaller size, lower aggregation number and shorter coronas than those generated from the aggregation of a copolymer

E-mail address: a.patti@uu.nl.

with approximately the same molecular weight and composition. On the other hand, they did not observe significant differences with the structure of the micelles obtained from the aggregation of the corresponding single arms.

Thanks to computer simulations, in the last two decades it has been possible to increase the level of understanding of the physics behind the formation of micelles in various types of amphiphilic solutions [31,32]. Molecular Dynamics [33–35], Brownian Dynamics [33], Dissipative Particle Dynamics [36,37], and Monte Carlo simulations [38–41], have been applied to study the phase and aggregation behavior of block copolymers. Most of these simulation techniques were performed on simplified models to handle the usual time and length scales involved in soft matter as detailed atomistic models are often too computationally demanding [42]. Coarse-grain models significantly reduce the number of atoms or molecules in the systems and the relative interactions established by grouping them together in a simplified manner [43]. Recently, Sheng et al. performed Dissipative Particle Dynamics (DPD) to compare the equilibrium structures of $(AB)_n$ and $(BA)_n$ star-block copolymers in a selective solvent for the A block [44]. Interestingly, they detected unimolecular micelles made of $(BA)_n$ stars, which are very similar to those observed in systems containing linear diblock AB copolymers. They showed that star-block copolymers can form uni- or supramolecular micelles according to (i) the distribution of the solvophobic and solvophilic units in the arms, (ii) their relative length, and (iii) the number of arms. In particular, for an $(AB)_n$ star in a good solvent for B , the uni- or supramolecular micellization strictly depends on the ability of B units to properly shield the solvophobic A -core from the contact with the solvent. This ability is a consequence of the delicate balance between the strength of AA , AB , and BB interactions, and the conformational entropy of the polymer. Unimolecular micelles can represent a significant improvement as drug delivery vehicles over multimolecular copolymer micelles. The covalent bond between the amphiphilic arms in unimolecular aggregates ensures a higher thermodynamic stability with respect to a micelle formed by distinct linear blocks, and reduces the probability to release the drug molecules to the surrounding solution. Because of their dynamic equilibrium with the free chains in solutions, multimolecular micelles made up of linear block copolymers might not accomplish this important task entirely [45–47]. Unimolecular and multimolecular micelles have been also observed more recently by Chou et al., who applied the DPD method to analyze the effect of arm number and length, solvent quality, and block length ratio, on the mean aggregation number in solutions of $(AB)_n$ star-block copolymers [48]. Jo and coworkers applied Brownian Dynamics simulations and a mean field theory to study the effect of the number of arms on the aggregation behavior of an $(AB)_n$ star-shaped copolymer, modeled as a bead-spring chain, in a selective solvent for the B block [49]. They found that the CMC shows a minimum when plotted as a function of the arm number, representing the optimal compromise between the entropic loss due to steric constraints in the micellar state, and large interfacial areas exposed to the solvent in the singly dispersed state.

In this work, we perform Monte Carlo simulations to study the aggregation behavior of a model star-block copolymer of general formula $(AB)_n$, with $n = 5$, in a selective solvent for the terminal B -group. We aim to understand how the main features of the self-assembly of this copolymer in micellar structures can be affected by the temperature, concentration, and by the solvophobic/solvophilic ratio of the block lengths. To this end, we model three different star-block copolymers whose block lengths ratio ranges from 0.5 to 2 and analyze their micellization properties. Moreover, we compare our simulation results with the recent theoretical model proposed by Kim and Lim, which provides the dependence of the CMC on the temperature [50]. By means of such a correlation, we could

estimate the standard free energy of micellization and analyze the thermodynamics behind the formation of micelles. In this context, we discuss the dual enthalpic–entropic nature of the driving force leading to the self-assembly of star-block copolymers.

The paper is organized as follows. In the next two sections, we describe the coarse-grained model and the simulation methodology applied, with a particular focus on the techniques used to study the aggregation properties of the micelles in equilibrium. In Section 4, we present and discuss the aggregation behavior and the thermodynamics of micellization by comparing the three architectures analyzed on the basis of their block length ratios. Finally some conclusions wrap up the paper.

2. Model

The coarse-grained model used in this paper was originally proposed by Larson who studied the aggregation behavior of linear surfactants in systems with oil and water [51]. In this model, the simulation box is organized into a three-dimensional cubic network of sites, and the amphiphilic chains are represented as sequence of connected beads. Each bead occupies a single site, and interacts with its nearest or diagonally-nearest neighbors along $z = 26$ directions, where z is the lattice coordination number. In our study, the amphiphilic star-like monomers occupy 31 sites, whereas the solvent occupies a single site. The monomers are composed of one central bead connected to five arms, as illustrated in Fig. 1. Each arm contains a solvophobic bridging group directly connected to the central bead, which is also solvophobic, and a solvophilic terminal group. The solvophobic and solvophilic beads are denoted by A and B , respectively. The solvent is denoted by S . Here, we use the abbreviation $A(A_xB_y)_5$ to indicate a star-block copolymer with five arms containing x solvophobic and y solvophilic beads, with $(x, y) = (3, 3), (4, 2),$ or $(2, 4)$.

The interaction between two beads i and j is given by the global interchange energy, ω_{ij} , which is the only relevant energetic parameter, and reads:

$$\omega_{ij} = \epsilon_{ij} - \frac{1}{2}(\epsilon_{ii} + \epsilon_{jj}) \quad (1)$$

with ϵ_{ij} being the individual interaction energies of a given pair of sites. We fixed the global interchange energies according to the main factors affecting the micellization process, which are (i) the repulsion of the solvophobic beads with the solvophilic beads and the solvent, and (ii) the solubility of the B beads in the solvent. In particular, $\omega_{AB} = 1$, $\omega_{AS} = 1$, and $\omega_{BS} = 0$. Note that from Eq. (1), $\omega_{ii} = 0$.

The dimensionless temperature reads

$$T^* = \frac{k_B T}{\omega_{AB}} \quad (2)$$

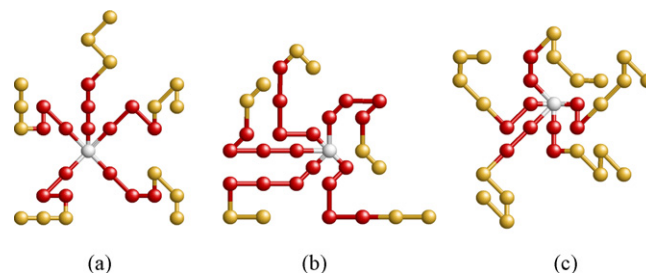


Fig. 1. Model star-block copolymers. $A(A_3B_3)_5$ (a); $A(A_4B_2)_5$ (b); $A(A_2B_4)_5$ (c). Solvophobic and solvophilic beads are in red and yellow, respectively. The central bead, in gray, is as solvophobic as any red bead. (For interpretation of the references to color in the figure caption, the reader is referred to the web version of the article.)

Table 1

Volume fractions, ϕ , number of stars, N_{stars} , and relative box size, L_{box} , of the systems studied.

ϕ (%)	0.01	0.025	0.05	0.1	0.25	0.5	1.0	3.0
N_{stars}	314	317	435	258	330	279	557	1672
L_{box}	460	340	300	200	160	120	120	120

where T is the absolute temperature and k_B the Boltzmann constant. For the three monomers represented in Fig. 1, different temperatures have been monitored, between $T^* = 4.0$ and $T^* = 12.0$.

3. Simulation methodology

We performed lattice Monte Carlo (MC) simulations at constant number of beads, volume and temperature (NVT ensemble), in a cubic box with periodic boundary conditions in the three dimensions. The volume of the box ranges from 120^3 to 460^3 , depending on the volume fraction of the chains, which ranges from $\phi = 0.01\%$ up to 5%. In Table 1, we give detailed information on the size of the simulation box at the concentrations studied. At lower concentrations than those listed in Table 1, the NVT ensemble becomes less efficient as a large system size would be required to ensure a sufficient number of monomers to form micelles. In these cases, a better choice would be to perform the simulations in the grand-canonical ensemble, where the chemical potential, rather than the number of monomers, is kept constant, as already shown in the study of self-assembling diblock and triblock copolymers [52,53].

The chains have been displaced by configurational bias moves, that is by partial and complete regrowth [54]. A typical mix of the MC moves used was 20% complete regrowth and 80% partial regrowth. In the equilibration run, all the simulations were carried out for at least 2×10^9 MC steps. This corresponds to a CPU time of roughly a week on a Dual-Core AMD Opteron Processor 2216, but denser systems needed up to two weeks to be equilibrated. The starting configurations consisted of chains sequentially placed on the lattice which were allowed to relax at a very high temperature ($T^* = 10^4$) for 2×10^5 MC steps. This created a completely random distribution of the chains and the initial configuration for the equilibration run. In the production run, we ensemble averaged the properties of the equilibrated systems 1000 times every 10^5 MC steps. At this stage, we computed the cluster size distribution, the radii of gyration, the density profiles through the micellar aggregates, and the critical micelle concentration.

3.1. Cluster size distribution

The computation of the cluster size distribution determines the average preferential size of the micellar aggregates and their dispersion in solution. Following the criterion used in previous works [41,55], an aggregate (or cluster) is defined as an assembly of monomers sharing at least one solvophobic bead as a neighbor. The cluster size distribution, $P(N)$, represents the average fraction of clusters of size N observed in the equilibrated solution during the production run. Using this definition, the average volume fraction of clusters containing N stars consisting of m beads is

$$\langle \phi_N \rangle = \frac{NmP(N)}{V} \quad (3)$$

where V is the volume of the simulation box and $\langle \dots \rangle$ denotes ensemble average. The peak of the cluster size distribution should not depend on the system size. If, by increasing the system size, a shift toward higher aggregation numbers is observed, this would be indicative of a phase separation, rather than a micellization. At the concentrations studied in this paper, we have never observed such a shifting.

3.2. Radii of gyration

The radii of gyration give information on the shape and size of the aggregates. They are obtained from the tensor of gyration [56]

$$R_{\alpha,\beta}^2 = \frac{1}{N_b} \sum_{k=1}^{N_b} (\alpha_k - \alpha_{cm})(\beta_k - \beta_{cm}) \quad (4)$$

where $\alpha, \beta = x, y, z$ are the three spatial directions, N_b is the number of beads in a given aggregate, and the subscript cm denotes the coordinate of the center of mass. The tensor of gyration can be diagonalized and its eigenvalues give the squares of the principal radii of gyration R_1, R_2 , and R_3 . In principle, if a given cluster had a perfect spherical shape, then the three radii would be identical. A useful single parameter to measure the deviation of the aggregates from the spherical shape is the so-called asphericity factor, defined as follows [56]:

$$A_d = \frac{\sum_{i>j}^d ((R_i^2 - R_j^2)^2)}{(d-1) \left(\sum_{i=1}^d R_i^2 \right)^2} \quad (5)$$

where d is the dimensionality of the system ($d = 3$ in our case). If the aggregate shows a perfect spherical shape, then A_d is equal to zero; otherwise it has a value between 0 and 1.

3.3. Composition profiles

To estimate the distribution of the beads, we calculated the composition profiles for concentric spherical shells around the center of the aggregate. The center of the aggregates was calculated as the center of mass of the cluster, giving equal weight to the beads of A and B blocks, and approximated to the nearest site in the lattice. Therefore, the composition profile $\rho_i(r)$ was obtained by counting the number of sites i in concentric shells of radius r , taking as the origin the cluster center, and dividing by the total number of sites in that concentric shell, considered as the volume of the shell, $V_s(r)$. $V_s(r)$ corresponds to the number of sites at a distance d , such that $r \leq d < r + 1$.

3.4. Critical micelle concentration

The CMC is the concentration at which micelles appear in the system. Well below the CMC, most of the amphiphilic stars is present as free monomers, and the concentration of micelles is practically negligible, although there is, in principle, a small probability of finding a cluster of any given size. As already done by other researchers [57,58], we assume that the CMC is the total concentration for which half of the surfactant is in aggregates of two or more amphiphiles. This corresponds to the concentration at which the curves of the free monomers and clusters concentration intersect.

4. Results

An illustrative sample of systems containing star-block copolymers above the CMC and hence forming micellar aggregates is shown in Fig. 2. Note the different box sizes and temperatures. As a general trend, the three star-block copolymers studied here are able to self-assemble in micellar aggregates. However, the range of temperatures at which this aggregation takes place is different and strictly related to the solvophobic/solvophilic block lengths ratio, ξ_{AB} , as we will show in this section.

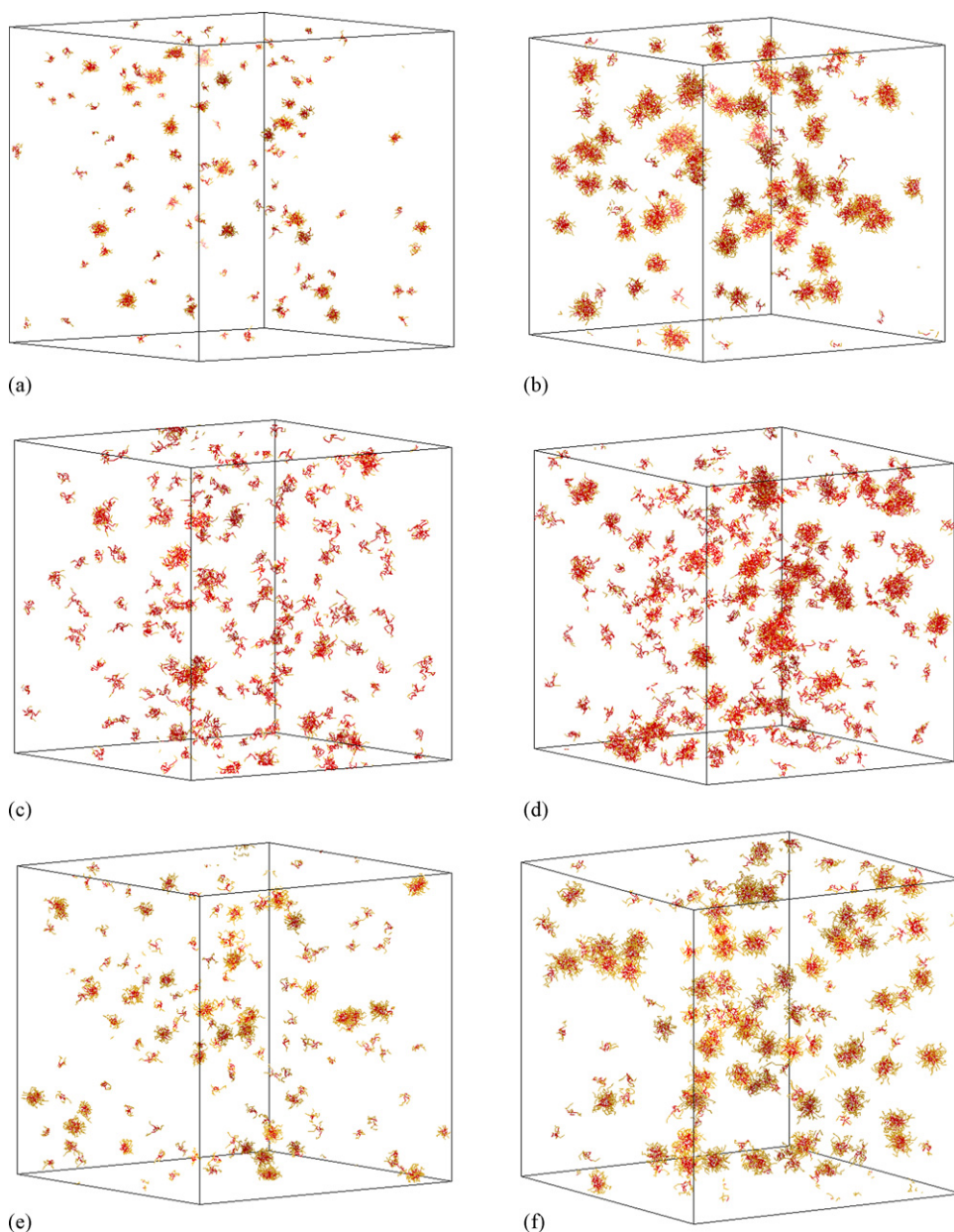


Fig. 2. Snapshots of micellar systems containing star-block copolymers. Top row: $A(A_3B_3)_5$ at $T^* = 8.0$; central row: $A(A_4B_2)_5$ at $T^* = 12.0$; bottom row: $A(A_2B_4)_5$ at $T^* = 6.0$. Concentrations and box volume: (a) $\phi = 0.1\%$ and $V = 200^3$; (b) $\phi = 1.0\%$ and $V = 120^3$; (c) $\phi = 0.5\%$ and $V = 120^3$; (d) $\phi = 1.0\%$ and $V = 120^3$; (e) $\phi = 0.25\%$ and $V = 160^3$; (f) $\phi = 1.0\%$ and $V = 120^3$. The A and B blocks are in red and yellow, respectively. (For interpretation of the references to color in the figure caption, the reader is referred to the web version of the article.)

In Fig. 3, we show the cluster size distribution (CSD) in one of the systems studied, which contains $A(A_3B_3)_5$ at $T^* = 8.0$. As soon as the concentration is raised above 0.05%, the CSD starts to develop a peak, which gives clear evidence of the presence of aggregates. The most probable size of such aggregates is $N_{max} = 10$, regardless the amphiphilic concentration of the system. The CMC, which will be estimated more precisely later on, must be located in between 0.05% and 0.1%. At the highest concentrations, a long tail is observed with a weak second peak located around $N = 20$. This does not indicate the presence of clusters with high aggregation number, but rather the inability of the algorithm used to distinguish between two separate aggregates in contact at a given point, and hence the probability of their solvophobic cores to touch each other (see the snapshot of two micelles touching each other in Fig. 3).

Due to the micellar nature of the solution, the location of the peak in the CSD does not show any significant depen-

dence on the amphiphilic concentration. However, it is strongly affected by the temperature and, more precisely, by the balance between two opposing contributions which are temperature-dependent: (i) the attraction between the solvophobic blocks, which is the main driving force for micellization, and (ii) the repulsion of the solvophilic groups, which becomes dominant at high temperatures and leads the system toward a more favorable disordered phase of free stars. When the temperature is increased, the aggregation number does not grow any further, but smaller micelles are more probable to be observed. Such an interplay determines the profiles shown in Fig. 4, which give the dependence of the most probable micellar size, N_{max} (that is the location of the peak in the CSD) on the temperature. In the three cases, we observe a peak which is approximately located at $T^* = 5.5, 8.2,$ and 10.2 for $A(A_2B_4)_5, A(A_3B_3)_5,$ and $A(A_4B_2)_5$, respectively.

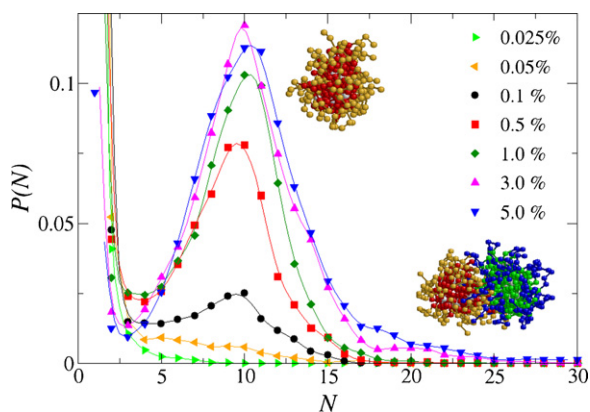


Fig. 3. Cluster size distribution of $A(A_3B_3)_5$ at $T^* = 8.0$ and different concentrations. Snapshots of an isolated micelle of 10 stars and two touching micelles of 9 and 11 stars are shown for $\phi = 5\%$. The solvophilic and solvophobic blocks of the micelle with 11 stars are in blue and green, respectively. The solid lines are a guide for the eyes. (For interpretation of the references to color in the figure caption, the reader is referred to the web version of the article.)

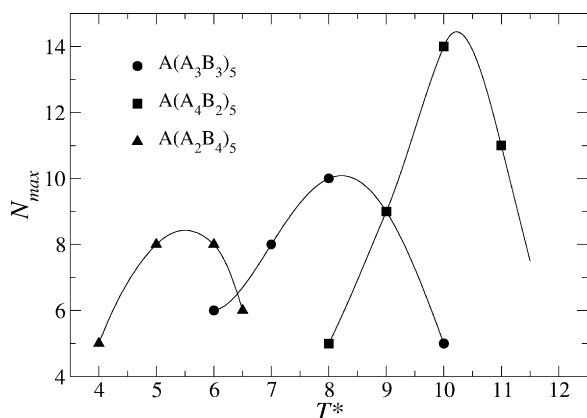


Fig. 4. Effect of the temperature on the peak of the CSDs in amphiphilic solutions of the star-block copolymers indicated in the legend. The solid lines are a guide for the eyes.

Insight on the shape of the clusters, whose size distribution is reported in Fig. 3, is provided by computing the radii of gyration or, equivalently, the asphericity factor A_d . In Fig. 5, we show A_d as a function of the aggregation number N at $T^* = 8.0$. For $N = N_{max}$,

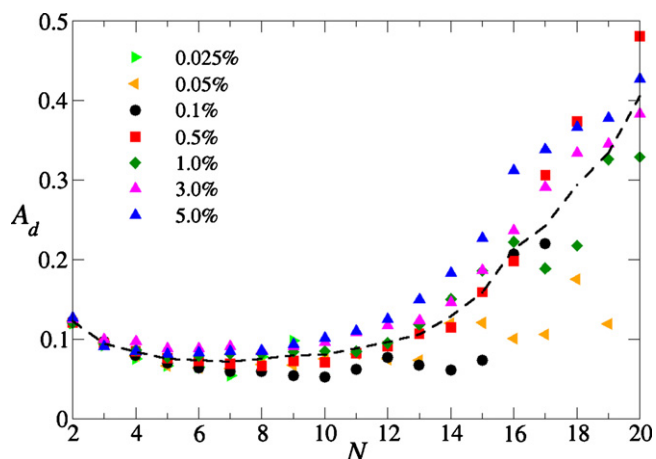


Fig. 5. Asphericity factors of the clusters observed in the system containing $A(A_3B_3)_5$. The dashed line represents the average between the asphericity factors at different concentrations. $T^* = 8.0$.

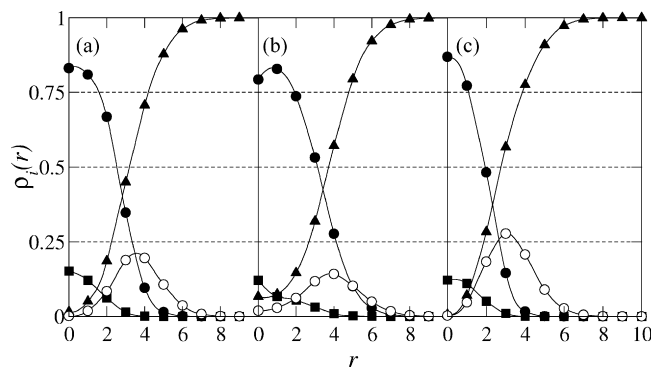


Fig. 6. Composition profiles in typical spherical aggregates observed in systems containing (a) $A(A_3B_3)_5$ at $T^* = 8.0$; (b) $A(A_4B_2)_5$ at $T^* = 10.0$; and (c) $A(A_2B_4)_5$ at $T^* = 5.0$. The amphiphile concentration is 0.1% in the three cases, whereas the aggregation number from left to right is 10, 14, and 8. Symbols: A-units (●); B-units (○); central bead (■); solvent (▲). The solid lines are a guide for the eyes.

we determined that $0.05 < A_d < 0.10$, which, with good approximation, implies the presence of spherical-shaped micelles. Slightly smaller or bigger aggregates still preserve a quasi-spherical shape. However, at $N > 15$, the asphericity factor increases (as well as the associated statistical noise) as a result of the temporary coalescence of different clusters. By changing the temperature, we did not detect any significant effect on the shape of the micelles which still preserve a quasi-spherical shape. Similar results have been also observed in systems containing $A(A_4B_2)_5$ or $A(A_2B_4)_5$ and are not shown here.

In Fig. 6, we display the density distribution profiles in micelles made of $A(A_3B_3)_5$, $A(A_4B_2)_5$, or $A(A_2B_4)_5$ at the same concentration ($\phi = 0.1\%$), and at those temperatures corresponding to the peaks of N_{max} in Fig. 4. The three profiles do not present any relevant distinctive feature, but those related to the number of stars per micelle, which is 10, 14, and 8 for $A(A_3B_3)_5$, $A(A_4B_2)_5$, and $A(A_2B_4)_5$, respectively. The inner core of the micelles is almost completely occupied by the solvophobic A-units, with the central beads preferentially located in the center. The peak of ρ_B is roughly located between three and four lattice units, where the penetration of the solvent is already quite significant. The B-units form a solvophilic corona which protects the solvophobic core from contact with the solvent. This task seems to be more effectively accomplished when the B block is formed by four beads (Fig. 6c), whereas a short solvophilic terminal group can leave some solvent to enter the core. It might be argued that, at a given temperature, higher aggregation numbers could provide further shielding against the penetration of the solvent in the micellar core. This scenario would imply a loss in the configurational entropy of the solvophobic blocks due to steric impediments, and would be thermodynamically unfavored. As a consequence, micelles with different aggregation numbers do not show any significant deviation in their density distribution profiles, which is indeed what we observed in our simulations and in a previous work [41].

By visual inspection, it is possible to appreciate how the single stars organize and orientate in the micellar aggregates. In Fig. 7, a typical micelle of $A(A_3B_3)_5$ is observed for $\phi = 5\%$ and $T^* = 8.0$. Interestingly, there is not a general preferential distribution of the chains: the solvophilic blocks belonging to the same star can be very close to each other (snapshots (b, c, and d)) or separated by the inner solvophobic core (snapshots (e and f)). As a consequence of this behavior, the central beads do not exclusively arrange in the inner region of the solvophobic core, but also closer to the border with the solvophilic corona, as confirmed by their quite broad density distribution profile of Fig. 6 (solid squares).

We defined the CMC as the concentration at which the amphiphilic moiety is equally distributed among free stars and

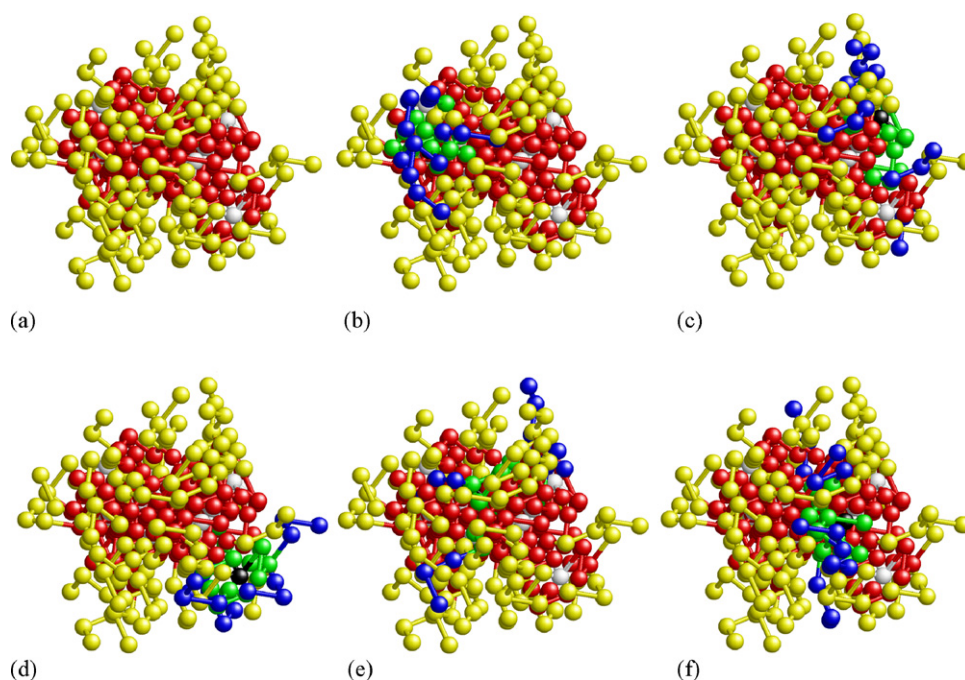


Fig. 7. Snapshots of an $A(A_3B_3)_5$ spherical micelle containing ten stars at $T^* = 8.0$ and $\phi = 5\%$. In snapshot (a) all the chains are represented as in Fig. 1(a). In each of the snapshots (b–f), one of the chains is highlighted to appreciate its orientation in the micelle: central bead in black, A-units in green, and B-units in blue. (For interpretation of the references to color in the figure caption, the reader is referred to the web version of the article.)

clusters, and it is given by the intercept between the concentration profile of the free stars and that of the clusters as a function of the total amphiphilic concentration (see Fig. 8). The values of the CMC as a function of temperature are given in Table 2. We note that Chen and Smid studied the micellization of star polymers with poly(ethylene oxide) arms in water solutions and estimated the CMC in the order of 10^{-3} M [5]. More recently, Lim et al. estimated that the CMC of poly(THF)-*b*-polyglycerol star copolymer is approximately 2.4×10^{-3} g/L [59]. The three star-block copolymers studied here show an increasing CMC with the temperature, as already observed for different linear block copolymers [53]. Moreover, increasing the ratio between the solvophobic and solvophilic blocks from $\xi_{AB} = 1$ to $\xi_{AB} = 2$, reduces the CMC by one or two orders of magnitude at the same temperature. At $T^* = 10.0$, for instance, the CMC of $A(A_3B_3)_5$ is 1.03%, whereas the CMC of $A(A_4B_2)_5$ is $3.17 \times 10^{-2}\%$. This result is due to the screening action in the

singly dispersed state exerted by the solvophilic B blocks on the solvophobic A blocks. The efficiency of such a shielding results to be significantly reduced when the length of the soluble block gets shorter, and, as a consequence, the tendency for stars to self-assemble rises. For similar reasons, if $\xi_{AB} = 1/2$, which is the case of the star-block copolymer $A(A_2B_4)_5$, the tendency to aggregate decreases and the CMC increases accordingly.

In Fig. 9, we plot the CMC as a function of the reduced temperature. As a general behavior, in the range of our simulation results, the CMC increases with increasing T^* . We note that in their experimental work on the micellization of PS/poly(2-vinylpyridine) star copolymer in a selective solvent for PS, Voulgaris et al. found an analogous exponential dependence of the CMC on temperature, which ranges from 2×10^{-4} g/cm³ at 294 K to 3×10^{-2} g/cm³ at 312 K [29]. Recently, Kim and Lim developed a theoretical framework describing the temperature dependence of the CMC by applying a straightforward thermodynamic scheme [50], based on (i) the closed association model, which assumes the monodispersity of micelles; (ii) the linear behavior of the enthalpy with the entropy of micellization (enthalpy–entropy compensa-

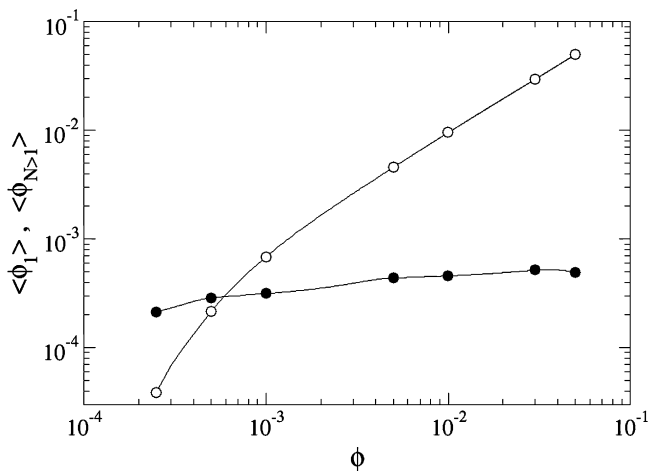


Fig. 8. Concentrations of free stars, ϕ_1 (solid circles), and clusters, $\phi_{N>1}$ (open circles), as a function of the total amphiphilic concentration of $A(A_3B_3)_5$ at $T^* = 8.0$. The intersection gives $\phi_{CMC} \approx 0.059\%$.

Table 2
Critical micelle concentrations, ϕ_{CMC} , at different temperatures.

Star-block copolymer	T^*	ϕ_{CMC} (%)
$A(A_3B_3)_5$	8.0	5.86×10^{-2}
	8.5	1.55×10^{-1}
	9.0	3.42×10^{-1}
	9.5	6.68×10^{-1}
	10.0	1.03
$A(A_4B_2)_5$	10.0	3.17×10^{-2}
	10.5	7.78×10^{-2}
	11.0	1.61×10^{-1}
	11.5	2.84×10^{-1}
	12.0	4.56×10^{-1}
$A(A_2B_4)_5$	5.5	3.43×10^{-2}
	6.0	1.60×10^{-1}
	6.5	5.15×10^{-1}
	7.0	1.24

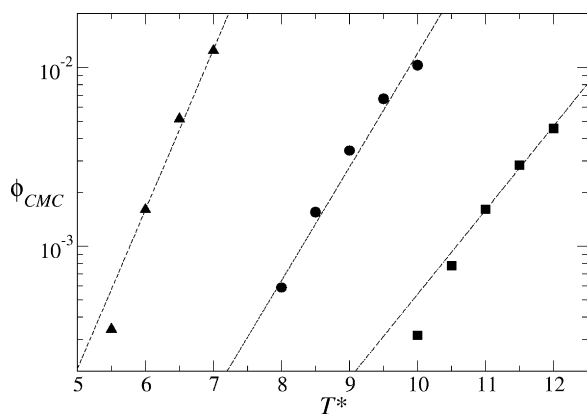


Fig. 9. Dependence of the critical micellar concentration on temperature. The dashed lines refer to the theoretical predictions according to Eq. (6) with the fitting constants of Table 3. The symbols represent our simulation results. (●) $A(A_3B_3)_5$; (▲) $A(A_4B_2)_5$; (■) $A(A_2B_4)_5$.

tion phenomenon [60]; and (iii) the Gibbs–Helmholtz equation. In particular, these authors found that

$$\ln \phi_{CMC} = A + BT + \frac{C}{T} \quad (6)$$

where A , B , and C are fitting constants proportional to $\Delta C_{p,mic}^0$, the change in the heat capacity of micellization [50]. We fitted our simulation results by applying Eq. (6) with the constants given in Table 3, and found a good quantitative agreement, although the micellar size distributions of the three copolymers at concentrations around the CMC are not as narrow as those typical of a monodisperse system. The sign of the fitting constants implies that the heat capacity decreases with increasing temperature. Moreover, since $\Delta C_{p,mic}^0 = \delta \Delta H_{mic}^0 / \delta T$, the change of the heat of micellization with the temperature is also negative, as will be shown later on. Generally speaking, the sign of the heat capacity is the result of two balancing effects. In aqueous solutions, a negative contribution to $\Delta C_{p,mic}^0$ arises from the change of the surface area of the hydrocarbon chains in contact with water, and it is due to the destruction of the water structure surrounding the solvophobic groups of the amphiphilic molecules upon micellization [61]. On the other hand, a positive contribution to $\Delta C_{p,mic}^0$ is associated to the reduction of the surface area available for the contact between the hydrophilic groups and water [62]. Usually, the first contribution is very significant as the hydrophobic interactions established upon micellization represent the dominant effect stabilizing the formation of aggregates. It follows that, on increasing the length of the hydrocarbon chain, the change in the heat capacity of micellization becomes more negative, as observed by Perger and Bešter-Rogač for different types of surfactants [63]. In such systems, the reduction of the contact area between the solvent and the solvophilic blocks, is generally negligible compared to the hydrophobic effect, and $\Delta C_{p,mic}^0$ is negative. However, amphiphiles with a different architecture, such as triblock copolymers, where the size of the terminal solvophilic blocks may be relevant with respect to that of the bridging solvophobic one, show a positive change of the heat capacity in a given range of temperatures, as recently observed for Pluronic F68 and F88 [62].

Table 3

Fitting constants of Eq. (6) for the three star-block copolymers indicated.

Star-block copolymer	A	B	C
$A(A_3B_3)_5$	−19.33	1.48	1.20
$A(A_4B_2)_5$	−18.46	1.09	0.27
$A(A_2B_4)_5$	−19.38	2.11	1.80

At those temperatures studied with simulations, the CMC of $A(A_4B_2)_5$ is lower than that of the other two star copolymers. This behavior is expected as the solvophobic blocks are longer and the ability to shield them from the contact with the solvent is relatively limited in free stars with a short solvophilic block. As the B block length increases (and, accordingly, the A block length decreases) this task is more easily accomplished and the resulting CMC is higher. The limit of such a behavior, corresponding to a star-block copolymer with a relatively large solvophilic block, is the difficulty to develop multimolecular micelles due to the steric repulsions established between the dense solvophilic coronas [44].

From the CMC and its dependence on the temperature, it is possible to describe and analyze the thermodynamics of micelle formation. More specifically, the change in the standard free energy of micellization, ΔG_{mic}^0 , depends on the concentration of free star-block copolymers at equilibrium with the micellar aggregates. Such a concentration can be safely considered equivalent to the CMC as it does not undergo significant changes at the free stars–micelles coexistence. The thermodynamic relation between the standard free energy of micellization and the CMC has been developed by the following two distinct trajectories. In the first, the micellization is considered as an equilibrium phenomenon described by the mass action law [64], whereas in the second the micelle is treated as a separate phase in equilibrium with free amphiphiles [65]. In both cases, the resulting dependence of the Gibbs free energy on the CMC can be expressed as:

$$\frac{\Delta G_{mic}^0}{k_B T} = \ln \phi_{CMC} \quad (7)$$

This equation has been derived for non-ionic surfactants and it can be applied to the systems studied here as no ions have been included in the coarse-grained model. It should be noted that Eq. (7) is valid under the assumption of large aggregation numbers. In our systems, the number of stars per micelle is not higher than ~ 12 , but if we think of a star as a group of amphiphilic chains, than the average aggregation number of such chains is five times bigger and the theoretical framework still holds.

From Eq. (7), the enthalpy of micellization is obtained by applying the Gibbs–Helmholtz equation:

$$\Delta H_{mic}^0 = -T^2 \frac{\delta \Delta G_{mic}^0 / T}{\delta T} = -k_B T^2 \frac{\delta \ln \phi_{CMC}}{\delta T} \quad (8)$$

The enthalpy of micellization can be calculated numerically by substituting Eq. (6) into Eq. (8):

$$\frac{\Delta H_{mic}^0}{k_B T} = -BT + \frac{C}{T} \quad (9)$$

Finally, the entropy of micellization, ΔS_{mic}^0 , can be determined by

$$T \Delta S_{mic}^0 = \Delta H_{mic}^0 - \Delta G_{mic}^0 \quad (10)$$

In Fig. 10, we show the temperature dependence of ΔG_{mic}^0 , ΔH_{mic}^0 , and $T \Delta S_{mic}^0$ in units of $k_B T$ for the three star-block copolymers. The shaded area refers to the range of temperatures at which we performed our simulations, which is $4.0 \leq T^* \leq 12.0$. The remaining part of the plot is the theoretical prediction at low and high temperatures not explored by simulations. As already discussed above, our simulation technique would be of little efficiency at $T^* < 4.0$, as the small values of the CMC would require a significantly big simulation box in order to sample the configurational space properly. It should be noted that the basic assumptions of the theory may not hold at very low temperatures where the systems are expected to solidify. Further investigation is needed to address this point, which is behind the scope of the present work, in more accurate detail. From the analysis of the enthalpy

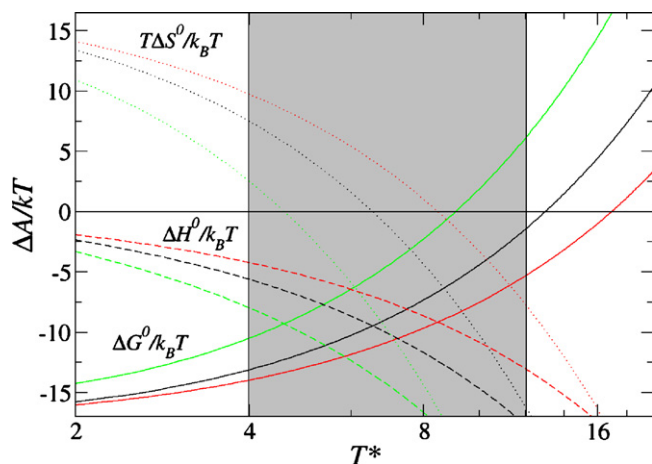


Fig. 10. Thermodynamic properties of micellization in systems of star-block copolymers. ΔA refers to the change in the free energy (solid lines), enthalpy (dashed lines), or entropy (dotted lines) of micellization. The thermodynamic properties referring to $A(A_3B_3)_5$, $A(A_4B_2)_5$, and $A(A_2B_4)_5$, are denoted by black, red, and green lines, respectively. The shaded area indicate the region where we performed simulations. (For interpretation of the references to color in the figure caption, the reader is referred to the web version of the article.)

of micellization, we can conclude that the micelle formation is an exothermic process ($\Delta H_{mic}^0 < 0$). At low temperatures, the negative value of the standard free energy is due to the large entropic contribution which overcomes the enthalpic term and drives the micelle formation. Such a positive change in the entropy upon micellization should be related to the configurational entropy of the solvophobic blocks, which assume a higher number of configurations when removed from the solution and incorporated in the micellar solvophobic cores. By approaching higher temperatures, the entropic term progressively decreases and the driving force for micellization assumes an enthalpic nature. At significantly high temperatures, the formation of micelles is not thermodynamically favored ($\Delta G_{mic}^0 > 0$) and star-block copolymers exist in solution in their singly dispersed state. This is detected at $T^* \approx 9.0, 13.0$ and 17.0 for $A(A_2B_4)_5$, $A(A_3B_3)_5$, and $A(A_4B_2)_5$, respectively.

5. Conclusions

In summary, we have studied the aggregation behavior of three star-block copolymers $(AB)_n$, with $n = 5$, whose block lengths ratio ranges from 0.5 to 2. In dilute solutions of a B -selective solvent, these systems are able to form micelles whose properties gradually change with the temperature. In particular, we found that the most probable aggregation number (the peak in the cluster size distribution) increases with the temperature up to a maximum and then decrease. The shape of the observed micelles is not significantly affected by temperature changes, but it keeps a (quasi) spherical geometry. On the other hand, the average number of stars per micelle shows a maximum if plotted as a function of temperature. Up to this maximum, the entropic contribution, which arises from the hydrophobic effect, drives the micelle formation and the aggregates grow in size. At the maximum, the entropic term is basically negligible and the micellar size does not grow any further.

The values of the CMC obtained by performing computer simulations have been compared with those predicted by a theory describing the dependence of the CMC on the temperature [50]. Although this theory assumes the monodispersity of the micelles in solution, and the cluster size distribution calculated at concentrations close to the CMC is not particularly narrow, we still found a good agreement, which, nevertheless, should be further verified with simulations at very low temperatures, that is $T^* < 4.0$ for the

three star-block copolymers studied here. We did not perform simulations at such low temperatures, because a significantly bigger simulation box would be required to sample a very dilute system. In this case, the μVT ensemble, at constant chemical potential, volume and temperature, would be more efficient.

By applying the relation between the CMC and the change in the standard free energy, we have determined the thermodynamic properties of micellization. The formation of micelles was found to be an entropy-driven process at low temperatures, where its exothermic nature is counterbalanced by an increase of configurational entropy of the solvophobic chains. At high temperatures, the process first becomes energy-driven as the entropic contribution fades out, and finally thermodynamically unstable, with $\Delta G_{mic}^0 > 0$.

Acknowledgements

The author gratefully acknowledges A.D. Mackie for critically reading the manuscript and a postdoctoral fellowship from Utrecht University.

References

- [1] W. Hamley, *The Physics of Blocks Copolymers*, Oxford University Press, Oxford, 1998.
- [2] P.R. Desai, N.J. Jain, R.K. Sharma, Effect of additives on the micellization of PEO/PPO/PEO block copolymer F127 in aqueous solution, *Colloids Surf. A: Physicochem. Eng. Asp.* 178 (2001) 57–69.
- [3] N.J. Jain, V.K. Aswal, P.S. Goyal, P. Bahadur, Salt induced micellization and micelle structures of PEO/PPO/PEO block copolymers in aqueous solution, *Colloids Surf. A: Physicochem. Eng. Asp.* 173 (2000) 85–94.
- [4] M. Szwarc, Living polymers. Their discovery, characterization, and properties, *J. Polym. Sci. Part A Polym. Chem.* 36 (1998) ix–xv.
- [5] X. Chen, J. Smid, Micellization of and solute binding to amphiphilic poly(ethylene oxide) star polymers in aqueous media, *Langmuir* 12 (1996) 2207–2213.
- [6] S.Y. Park, D.K. Han, S.C. Kim, Synthesis and characterization of star-shaped PLLAPEO block copolymers with temperature-sensitive sol-gel transition behavior, *Macromolecules* 34 (2001) 8821–8824.
- [7] M. Yoo, A. Heise, J.L. Hedrick, R.D. Miller, C.W. Frank, Photophysical characterization of conformational rearrangements for amphiphilic 6-arm star block copolymers in selective solvent mixtures, *Macromolecules* 36 (2003) 268–271.
- [8] S.Y. Park, B.R. Han, K.M. Na, D.K. Han, S.C. Kim, Micellization and gelation of aqueous solutions of star-shaped PLLAPEO block copolymers, *Macromolecules* 36 (2003) 4115–4124.
- [9] K. Min, H. Gao, K. Matyjaszewski, Preparation of homopolymers and block copolymers in miniemulsion by ATRP using activators generated by electron transfer (AGET), *J. Am. Chem. Soc.* 127 (2005) 3825–3830.
- [10] W. Jakubowski, K. Matyjaszewski, Activator generated by electron transfer for atom transfer radical polymerization, *Macromolecules* 38 (2005) 4139–4146.
- [11] J.K. Oh, R. Drumright, D.J. Siegwart, K. Matyjaszewski, The development of microgels/nanogels for drug delivery applications, *Prog. Polym. Sci.* 33 (2008) 448–477.
- [12] H.J. Jeon, D.H. Go, S.-Y. Choi, K.M. Kim, J.Y. Lee, D.J. Choo, H.-O. Yoo, J.M. Kim, J. Kim, Synthesis of poly(ethylene oxide)-based thermoresponsive block copolymers by RAFT radical polymerization and their uses for preparation of gold nanoparticles, *Colloids Surf. A: Physicochem. Eng. Asp.* 317 (2008) 496–503.
- [13] M. Pitsikalis, S. Pispas, J.W. Mays, N. Hadjichristidis, Nonlinear block copolymer architectures, *Adv. Polym. Sci.* 135 (1998) 1–137.
- [14] M. Meier, J.-F. Gohy, C.-A. Fustin, U. Schubert, Combinatorial synthesis of star-shaped block copolymers: host guest chemistry of unimolecular reversed micelles, *J. Am. Chem. Soc.* 126 (2004) 11517–11521.
- [15] R. Haag, Supramolecular drug-delivery systems based on polymeric core-shell architectures, *Angew. Chem., Int. Ed.* 43 (2004) 278–282.
- [16] M. Liu, K. Kono, J.M.J. Frechet, Water-soluble dendritic unimolecular micelles: their potential as drug delivery agents, *J. Control. Release* 65 (2000) 121–131.
- [17] T. Ooya, J. Lee, K. Park, Effects of ethylene glycol-based graft, star-shaped, and dendritic polymers on solubilization and controlled release of paclitaxel, *J. Control. Release* 93 (2003) 121–127.
- [18] F. Wang, T.K. Bronich, A.V. Kabanov, R.D. Rauh, J. Roovers, Synthesis and evaluation of a star amphiphilic block copolymer from poly(ϵ -caprolactone) and poly(ethylene glycol) as a potential drug delivery carrier, *J. Bioconjug. Chem.* 16 (2005) 397–405.
- [19] P.W. Dong, X.H. Wang, Y.C. Gu, Y.J. Wang, Y.J. Wang, C.Y. Gong, F. Luo, G. Guo, X. Zhao, Y.Q. Wei, Z.Y. Qian, Self-assembled biodegradable micelles based on star-shaped PCL-b-PEG copolymers for chemotherapeutic drug delivery, *Colloids Surf. A: Physicochem. Eng. Asp.* 358 (2010) 128–134.
- [20] S. Anastasiadis, H. Retsos, S. Pispas, N. Hadjichristidis, S. Neophytides, *Smart Polym. Surf., Macromolecules* 36 (2003) 1994–1999.

- [21] T. Terashima, M. Kamigaito, K.-Y. Baek, T. Ando, M. Sawamoto, Polymer catalysts from polymerization catalysts: direct encapsulation of metal catalyst into star polymer core during metal-catalyzed living radical polymerization, *J. Am. Chem. Soc.* 125 (2003) 5288–5289.
- [22] A.W. Bosman, R. Vestberg, A. Heumann, J.M.J. Frechet, C.J. Hawker, A modular approach toward functionalized three-dimensional macromolecules: from synthetic concepts to practical applications, *J. Am. Chem. Soc.* 123 (2003) 715–728.
- [23] C. Bouilhac, E. Cloutet, H. Cramail, A. Deffieux, D. Taton, Functionalized star-like polystyrenes as organic supports of a tridentate bis(imino)pyridinyliron/aluminic derivative catalytic system for ethylene polymerization, *Macromol. Rapid. Commun.* 26 (2005) 1619–1625.
- [24] E.W. Merrill, Poly(ethylene oxide) star molecules: synthesis, characterization, and applications in medicine and biology, *J. Biomater. Sci. Polym. Ed.* 5 (1993) 1–11.
- [25] R. Knischka, P.J. Lutz, A. Sunder, R. Mulhaupt, H. Frey, Functional poly(ethylene oxide) multiarm star polymers: core-first synthesis using hyperbranched polyglycerol initiators, *Macromolecules* 33 (2000) 315–320.
- [26] G. Lapienis, Star-shaped polymers having PEO arms, *Prog. Polym. Sci.* 34 (2009) 852–892.
- [27] A. Blencowe, J.F. Tan, T.K. Goh, G.G. Qiao, Core cross-linked star polymers via controlled radical polymerisation, *Polymer* 50 (2009) 5–32.
- [28] S. Pispas, Y. Poulos, N. Hadjichristidis, Micellization behavior of $(PS)_8(PI)_8$ Miktoarm (Vergina) star copolymers, *Macromolecules* 31 (1998) 4177–4181.
- [29] D. Voulgaris, C. Tsitsilianis, F.J. Esselink, G. Hadziioannou, Polystyrene/poly(2-vinyl pyridine) heteroarm star copolymer micelles in toluene: morphology and thermodynamics, *Polymer* 39 (1998) 6429–6439.
- [30] G. Mountrichas, M. Mpiri, S. Pispas, Micelles of star block $(PSPI)_8$ and PSPI diblock copolymers (PS = polystyrene, PI = polyisoprene): structure and kinetics of micellization, *Macromolecules* 38 (2005) 940–947.
- [31] J.C. Shelley, M.Y. Shelley, Computer simulation of surfactant solutions, *Curr. Opin. Colloid Interface Sci.* 5 (2000) 101–110.
- [32] R. Rajagopalan, Simulations of self-assembling systems, *Curr. Opin. Colloid Interface Sci.* 6 (2001) 357–365.
- [33] M.A. Horsch, Z. Zhang, C.R. Iacovella, S.C. Glotzer, Hydrodynamics and microphase ordering in block copolymers: are hydrodynamics required for ordered phases with periodicity in more than one dimension? *J. Chem. Phys.* 121 (2004) 11455–11462.
- [34] X. Li, D. Kou, S. Rao, H. Liang, Developing a coarse-grained force field for the diblock copolymer poly(styrene-*b*-butadiene) from atomistic simulation, *J. Chem. Phys.* 124 (2006) 204909–204915.
- [35] D. Bedrov, C. Ayyagari, G.D. Smith, Multiscale modeling of poly(ethylene oxide)poly(propylene oxide)poly(ethylene oxide) triblock copolymer micelles in aqueous solution, *J. Chem. Theory Comp.* 2 (2006) 598–606.
- [36] R.D. Groot, T.J. Madden, Dynamic simulation of diblock copolymer microphase separation, *J. Chem. Phys.* 108 (1998) 8713–8724.
- [37] C. Soto-Figueroa, L. Vicente, J.M. Martanez-Magadn, M. Rodriguez-Hidalgo, Self-organization process of ordered structures in linear and star poly(styrene)-poly(isoprene) block copolymers: Gaussian models and mesoscopic parameters of polymeric systems, *J. Phys. Chem. B* 111 (2007) 11756–11764.
- [38] K. Binder, H. Fired, Asymmetric block copolymer melts near the microphase separation transition: a Monte Carlo simulation, *Macromolecules* 26 (1993) 6878–6883.
- [39] A. Hoffmann, J.U. Sommer, A. Blumen, Statistics and dynamics of dense copolymer melts: a Monte Carlo simulation study, *J. Chem. Phys.* 106 (1997) 6709–6721.
- [40] F.R. Siperstein, K.E. Gubbins, Phase separation and liquid crystal self-assembly in surfactant inorganic solvent systems, *Langmuir* 19 (2003) 2049–2057.
- [41] A. Patti, A.D. Mackie, F.R. Siperstein, Monte Carlo simulation of self-assembled ordered hybrid materials, *Langmuir* 23 (2007) 6771–6780.
- [42] M.L. Klein, W. Shinoda, Large-scale molecular dynamics simulations of self-assembling systems, *Science* 321 (2008) 798–800.
- [43] B. Smit, P.A. Hilbers, K. Esselink, L.A.M. Rupert, N.M. van Os, A.G. Schlijper, Computer simulations of a water/oil interface in the presence of micelles, *Nature* 348 (1990) 624–625.
- [44] Y.-J. Sheng, C.-H. Nung, H.-K. Tsao, Morphologies of star-block copolymers in dilute solutions, *J. Phys. Chem. B* 110 (2006) 21643–21650.
- [45] M. Gauthier, L. Tichagwa, J.S. Downey, S. Gao, Arborescent graft copolymers: highly branched macromolecules with a core-shell morphology, *Macromolecules* 29 (1996) 519–527.
- [46] H. Liu, A. Jiang, J.A. Guo, K.E. Uhrich, Unimolecular micelles: synthesis and characterization of amphiphilic polymer systems, *J. Polym. Sci. Part A: Polym. Chem.* 37 (1999) 703–711.
- [47] H. Liu, S. Farrell, K.E. Uhrich, Drug release characteristics of unimolecular polymeric micelles, *J. Control. Release* 68 (2000) 167–174.
- [48] S.-H. Chou, H.-K. Tsao, Y.-J. Sheng, Atypical micellization of star-block copolymer solutions, *J. Chem. Phys.* 129 (2008) 224902–224911.
- [49] J. Huh, K.H. Kim, C.-H. Ahn, W.H. Jo, Micellization behavior of star-block copolymers in a selective solvent: a Brownian dynamics simulation approach, *J. Chem. Phys.* 121 (2004) 4998–5007.
- [50] H.-U. Kim, K.-H. Lim, A model on the temperature dependence of critical micelle concentration, *Colloids Surf. A: Physicochem. Eng. Asp.* 235 (2004) 121–128.
- [51] R.G. Larson, L.E. Scriven, H.T. Davis, Monte Carlo simulation of model amphiphile-oil water systems, *J. Chem. Phys.* 83 (1985) 2411–2420.
- [52] M.A. Floriano, E. Caponetti, A.Z. Panagiotopoulos, Micellization in model surfactant systems, *Langmuir* 15 (1999) 3143–3151.
- [53] A.Z. Panagiotopoulos, A.M. Floriano, S.K. Kumar, Micellization and phase separation of diblock and triblock model surfactants, *Langmuir* 18 (2002) 2940–2948.
- [54] D. Frenkel, B. Smit, *Understanding Molecular Simulations: From Algorithms to Applications*, 2nd ed., Academic Press, San Diego, 2001.
- [55] A. Patti, A.D. Mackie, F.R. Siperstein, Monte Carlo simulations of self-assembling hexagonal and cage-like bifunctional periodic mesoporous materials, *J. Mater. Chem.* 19 (2009) 7848–7855.
- [56] J. Rudnick, G. Gaspari, The shapes of random walks, *Science* 237 (1987) 384–389.
- [57] D. Stauffer, N. Jan, Y. He, R.B. Pandley, D.G. Marangoni, T. Smith-Palmer, Micelle formation, relaxation time, and three-phase coexistence in a microemulsion model, *J. Chem. Phys.* 100 (1994) 6934–6943.
- [58] A.D. Mackie, A.Z. Panagiotopoulos, I. Szleifer, Aggregation behavior of a lattice model for amphiphiles, *Langmuir* 13 (1997) 5022–5031.
- [59] S.-H. Lim, E.-J. Cha, J. Huh, C.-H. Ahn, Micelle behavior of copolymers composed of linear and hyperbranched blocks in aqueous solution, *Macromol. Chem. Phys.* 210 (2009) 1734–1738.
- [60] D.F. Evans, Self-organization of amphiphiles, *Langmuir* 4 (1988) 3–12.
- [61] C. Tanford, *The Hydrophobic Effect: Formation of Micelles in Biological Membranes*, 2nd ed., Wiley-Interscience Publication, 1980.
- [62] H.-W. Tsui, Y.-H. Hsu, J.-H. Wang, L.-J. Chen, Novel behavior of heat of micellization of Pluronic F68 and F88 in aqueous solutions, *Langmuir* 24 (2008) 13858–13862.
- [63] T.-M. Perger, M. Bešter-Rogač, Thermodynamics of micelle formation of alkyltrimethylammonium chlorides from high performance electric conductivity experiments, *J. Colloids Interface Sci.* 313 (2007) 288–295.
- [64] J.N. Phillips, The energetics of micelle formation, *Trans. Faraday Soc.* 51 (1955) 561–569.
- [65] E. Matijević, B.A. Pethica, The heats of micelle formation of sodium dodecyl sulphate, *Trans. Faraday Soc.* 54 (1958) 587–592.